# HIGH-REYNOLDS NUMBER SCALE-RESOLVING SIMULATIONS OF AXISYMMETRIC DENSITY CURRENT

**Ricardo A. S. Frantz**
Laboratoire DynFluid
Arts et Métiers ParisTech,
151 Bd. de l'Hôpital, 75013 Paris, France
ricardo.frantz@ensam.eu

**Bruno A. Farenzena**
Escola Politécnica
Pontifícia Universidade Católica do Rio Grande do Sul
Av. Ipiranga 6681, 90619-900 Porto Alegre-RS, Brazil
bruno.farenzena@acad.pucrs.br

**Sylvain Laizet**
Department of Aeronautics
Imperial College London
London SW7 2AZ, United Kingdom
s.laizet@imperial.ac.uk

**Jorge H. Silvestrini**
Escola Politécnica
Pontifícia Universidade Católica do Rio Grande do Sul
Av. Ipiranga 6681, 90619-900 Porto Alegre-RS, Brazil
jorgehs@pucrs.br

## ABSTRACT

A three-dimensional implicit Large-Eddy simulation is presented for a cylindrical density current at a Reynolds number equal to $136,000$, under the Boussinesq approximation for small density difference. The aim is to assess the ability of an implicit Spectral Vanishing Viscosity approach to numerically reproduce the main features of an axisymmetric release of heavy fluid into a light ambient fluid at high Reynolds numbers. Comparisons are made with experimental data and with numerical data at lower Reynolds numbers. It is found that the proposed approach is able to provide a detailed description of the structure of the current, information about the large-scale coherent structures, and to predict the evolution of the front velocity over the different stages of the current propagation.

## INTRODUCTION

Turbulent density currents are produced when a finite volume of heavy fluid is released from a source into an ambient fluid with a lower density. They are very common in nature with seafloor turbidity currents, avalanches, haboobs, river plumes, pyroclastic and lava flows. Density currents have been studied in great details, using a combination of laboratory experiments, mathematical models, and numerical simulations. They exhibit a complex dynamic with the presence of the well-known lobe-and-cleft patterns at the head of the current followed by a region of mixing with intense Kelvin-Helmholtz vortices. Understanding the physical mechanism associated with these currents as well as the correct prediction of their main features are of great importance for practical and theoretical purposes. Studying density currents in nature is very challenging and costly due to their complexity and size. As a result, density currents are investigated in simplified and idealised configurations. The most studied one is the horizontal channelized lock-exchange configuration in which the heavy fluid is enclosed in a small reservoir separated by a gate from the light ambient fluid in a channel set-up. The dynamics of channelized density currents are reasonably well understood with a large number of experimental, numerical and theoretical studies as well as predictive models (see Simpson (1999); Meiburg & Kneller (2010) for a comprehensive overview of the study of density currents).

Recently, scale-resolving simulations (in which (most of) the turbulent scales are resolved) have been performed in two and three dimensions to explore the dynamics of density currents. Most of these simulations are dealing with channelized lock-exchange configuration (Härtel et al., 2000b,a; Necker et al., 2002; Espath et al., 2014) but some of them are also focusing on axisymmetric configurations however at relatively low Reynolds numbers (Cantero et al., 2006, 2007a; Zgheib et al., 2015). Scale-resolving simulations of lock-exchange density currents can be used to accurately estimate the temporal evolution of global parameters such as the front location and front velocity as well as the height of the current. Detailed information about the lobe-and-cleft structures and the deposition map can also be obtained from scale-resolving simulations, data which are almost impossible to get from experiments.

Direct Numerical Simulation (DNS) is probably the best option to study numerically density currents because of its ability to resolve all the scales of the flow (without any modelling). Unfortunately, it is not yet reasonable to perform DNS of density currents at high Reynolds numbers (of the order of $10^5$ and more), even with the most powerful supercomputers available for academic research. As a result, Large Eddy Simulations (LES), for which only the smallest scales of the flow are modelled, is a more suitable strategy. Interestingly, only few density currents studies are based on LES, even if LES is now a widely used technique in academia and industry for the study of turbulent flows at Reynolds numbers representative of real-life applications (see Constantinescu (2014) for an extensive review of LES of lock-exchange gravity currents). The vast majority of LES for density currents are focusing on channelized lock-exchange configuration and are based on explicit models to deal with the unresolved sub-grid scales. To the best of our knowledge, there is no published work of LES of density currents generated with cylindrical re-

leases. In the present study, the axisymmetric collapse of a heavy fluid column in a lighter environment for a high Reynolds number equal to 136,000 is studied by means of Implicit Large Eddy Simulation using the Boussinesq approximation for small density difference. This configuration has been chosen because experimental data are available for this Reynolds number (Hallworth *et al.*, 2001). The present study is based on an original approach based on a strategy that uses the numerical error of high-order implicit finite-difference scheme to introduce dissipation at small scales. It means that it is not necessary to use an explicit model for the unresolved sub-grid scales (there is no extra cost associated with the proposed approach). This strategy has been applied successfully to scale-resolving simulations of homogeneous isotropic turbulence (Dairay *et al.*, 2017), turbulent jets (Ioannou & Laizet, 2018) and the wake generated by wind turbines (Deskos *et al.*, 2019). The aim here is to assess the ability of this approach to reproduce at a reasonable cost the complexity of an axisymmetric density current at high Reynolds number, with some comparisons with experimental data. The selected experimental case (S3 in Hallworth *et al.* (2001)) was performed by quickly releasing a given cylindrical volume of dense salt water at the centre of a circular tank containing fresh ambient water.

## NUMERICAL METHODOLOGY

To describe the evolution of density currents, the three-dimensional incompressible Navier-Stokes equations, coupled with a scalar transport equation, are used under the Boussinesq approximation. The governing equations read

$$\frac{\partial u_i}{\partial x_i} = 0,$$

$$\frac{\partial u_i}{\partial t} = -u_j \frac{\partial u_i}{\partial x_j} - \frac{\partial p}{\partial x_i} + \frac{1}{Re} \frac{\partial^2 u_i}{\partial x_j \partial x_j} - \theta \delta_{i2},$$

$$\frac{\partial \theta}{\partial t} = -u_i \frac{\partial \theta}{\partial x_i} + \frac{1}{Re\,Sc} \frac{\partial^2 \theta}{\partial x_i \partial x_i} \qquad (1)$$

where $u_i$ is the velocity field, $p$ the pressure, $\theta$ the scalar concentration, $\delta_{ij}$ the Kronecker delta, $Re$ the Reynolds number and $Sc$ the Schmidt number equal to 1. All quantities describe the evolution of large scales of motion and buoyancy and are formally filtered by the computational mesh.

To describe the problem a single characteristic velocity scale (i.e. the buoyancy velocity) can be estimated assuming an inviscid energy budget, while the reference length scale is arbitrary chosen as the height of the heavy fluid column $\tilde{L}_{2,b}$ (see Fig. 3a for a visualisation of the flow configuration). Henceforth, the bulk Reynolds number is estimated as $Re = (g'\tilde{L}_{2,b}^3)^{0.5}/\nu$, where $g'$ represents the reduced density and $\nu$ the kinematic viscosity. In the following, $\tilde{L}_{2,b}$ and the buoyancy velocity are used for the normalisation of all quantities.

The simulation is performed with the open source flow solver `Incompact3d`, which is based on a Cartesian mesh, finite-difference 6th-order compact schemes for spatial discretisation and a 3rd-order Adams-Bashforth scheme for time-advancement. The main originality of `Incompact3d` is that the Poisson equation for the incompressibility of the velocity field is fully solved in spectral space via the use of relevant 3D Fast Fourier transforms (FFTs). With the help of the concept of modified
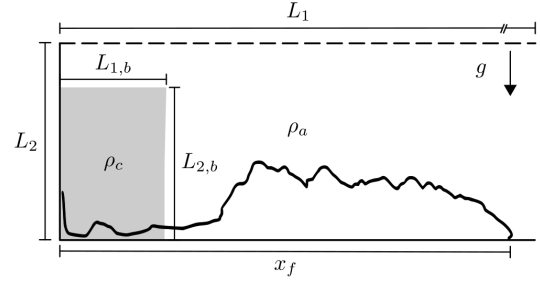


Figure 1.   2D Schematic view of the flow configuration.

wavenumber (Lele, 1992), the divergence-free condition is ensured up to machine accuracy. The pressure mesh is staggered from the velocity one by half a mesh to avoid spurious pressure oscillations observed in a fully collocated approach (Laizet & Lamballais, 2009). The simplicity of the mesh allows an easy implementation of a 2D domain decomposition based on pencils (Laizet & Li, 2011). The computational domain is split into a number of sub-domains (pencils) which are each assigned to an MPI-process. The derivatives and interpolations in the x-direction (y-direction, z-direction) are performed in X-pencils (Y-pencils, Z-pencils), respectively. The 3D FFTs required by the Poisson solver are also broken down as a series of 1D FFTs computed in one direction at a time. Global transpositions to switch from one pencil to another are performed with the MPI command `MPI_ALLTOALL(V)`. `Incompact3d` can scale well with hundreds of thousands MPI-processes for large-scale simulations (Laizet & Li, 2011).

Free-slip boundary conditions are applied for the velocity in the three spatial directions, except at the bottom wall where a no-slip boundary condition is imposed. Note that only 1/4 of the cylinder is simulated to save computational resources. For the scalar field, no-flux conditions are imposed everywhere. The initial condition is prescribed with a smooth hyperbolic tangent to avoid discontinuities. It is noteworthy that we ignore the inner cylinder which is present in the experimental setup (which results in an initial condition with 4.6% additional mass). High amplitude $O(15\%)$ white noise is superposed at the lock position to accelerate the breakdown to turbulence and to mimic the strong disturbance introduced by the removal of the lock in the experimental setup. A 2D schematic view of the flow configuration can be seen in figure 1. The simulation is performed in a dimensionless domain of $L_1 \times L_2 \times L_3 = 17 \times 1.6 \times 17$, with the scalar field prescribed radially for a quarter of cylinder with $L_{1,b} \times L_{2,b} = 2.2 \times 1$. The experiment length $L_{1,3} = 14.2$ in Hallworth *et al.* (2001) was increased to accommodate for an even longer spatiotemporal evolution of the current. The domain is discretised with $n_1 \times n_2 \times n_3 = 901 \times 389 \times 901$ uniform mesh nodes ($\sim 316$ million mesh nodes) and the time step of $\Delta t = 0.00024$ is kept constant throughout the simulation.

## Implicit LES

The proposed scale-resolving simulation is based on a strategy that introduces a targeted numerical dissipation at the small scales through the discretisation of the second derivatives of the viscous terms Lamballais *et al.* (2011); Dairay *et al.* (2017). It was shown in these studies that it is possible to design a 6th-order finite-difference scheme in or-

der to mimic a subgrid-scale model based on the concept of Spectral Vanishing Viscosity (SVV, see for instance Karamanos & Karniadakis (2000)), at no extra computational cost.

In `Incompact3d`, the computation of second derivatives is achieved thanks to the following scheme

$$\alpha f''_{i-1} + f''_i + \alpha f''_{i+1} = a\frac{f_{i+1} - f_i + f_{i-1}}{2\Delta x^2} + \\ b\frac{f_{i+2} - 2f_i + f_{i-2}}{4\Delta x^2} + \\ c\frac{f_{i+3} - 2f_i + f_{i-3}}{9\Delta x^2} + \\ d\frac{f_{i+4} - 2f_i + f_{i-4}}{16\Delta x^2}. \quad (2)$$

In the framework of a Fourier analysis, it is well known that a modified square wavenumber $k''$ can be related to this scheme with

$$k''\Delta x^2 = \frac{2a\left[1 - \cos(k\Delta x)\right] + \frac{b}{2}\left[1 - \cos(2k\Delta x)\right] +}{1 + 2\alpha\cos(k\Delta x)} \\ \frac{\frac{2c}{9}\left[1 - \cos(3k\Delta x)\right] + \frac{d}{8}\left[1 - \cos(4k\Delta x)\right].}{1 + 2\alpha\cos(k\Delta x)} \quad (3)$$

For a conventional 6th-order order scheme, the coefficients of the discretisation are $\alpha = 2/11$, $a = 12/11$, $b = 3/11$, $c = d = 0$. Using two conditions on the modified square wavenumber $k''$, one at the cutoff wavenumber ($k_c = \pi/\delta x$ with $k''|_\pi = k''_c$) and one at an intermediate scale $2\pi/3$ ($k''|_{2\pi/3}$ with $k''|_{2\pi/3} = k''_m$), the scheme 2 can produce the following set of coefficients

$$\alpha = \frac{1}{2} - \frac{320k''_m\Delta x^2 - 1296}{405k''_c\Delta x^2 - 640k''_m\Delta x^2 + 144}$$

$$a = -\frac{4329k''_c\Delta x^2/8 - 32k''_m\Delta x^2 - 140k''_c\Delta x^2 k''_m\Delta x^2 + 286}{405k''_c\Delta x^2 - 640k''_m\Delta x^2 + 144}$$

$$b = \frac{2115k''_c\Delta x^2 - 1792k''_m\Delta x^2 - 280k''_c\Delta x^2 k''_m\Delta x^2 + 1328}{405k''_c\Delta x^2 - 640k''_m\Delta x^2 + 144}$$

$$c = -\frac{7695k''_c\Delta x^2/8 + 288k''_m\Delta x^2 - 180k''_c\Delta x^2 k''_m\Delta x^2 - 2574}{405k''_c\Delta x^2 - 640k''_m\Delta x^2 + 144}$$

$$d = \frac{198k''_c\Delta x^2 + 128k''_m\Delta x^2 - 40k''_c\Delta x^2 k''_m\Delta x^2 - 736}{405k''_c\Delta x^2 - 640k''_m\Delta x^2 + 144}. \quad (4)$$

As explained in Lamballais *et al.* (2011), the extra-dissipation introduced by this discrete viscous operator can be interpreted as a spectral viscosity expressed as

$$v''_s = v\frac{k'' - k^2}{k^2}. \quad (5)$$

Using this expression, it is quite straightforward to adjust the coefficient in order to mimic the following SVV kernel

$$v_s(k) = v_0 \exp\left(-\left(\frac{k_c - k}{0.3k_c - k}\right)\right) \quad (6)$$

where $k_c$ is the cutoff wave number of the computational mesh and $v_0$ an artificial viscosity that controls the numerical extra-dissipation. For the present study, the two conditions $v''_s(k_c) = v_s(k)$ and $v''_s(2k_c/3) = v_s(2k/3)$ are imposed, with $v_0/v = 450$. This value has been obtained empirically after several preliminary simulations.

## RESULTS

Figure 2 presents instantaneous visualisations of the scalar $\theta$ at $t = 6.4$ and $t = 15.2$. When the lock is removed, the heavy fluid begins to collapse and spreads out radially into the light ambient fluid. The head of the current is characterised by rolled up vortices. When the current start to slow down, the well-known lobe-and-cleft structures start to emerge, however, because the Reynolds number is very high, they are quite small, in very large numbers and it is quite challenging to clearly identify them. It was already reported in Espath *et al.* (2014) that lobe-and-cleft structures reduce in size when the Reynolds number is increased. They are also not as well organised as for lower Reynolds number, suggesting a strong influence of the Reynolds number for this type of flow. Note that the maximum height of the current is located close to the head, where the current is slightly lifted away from the bottom wall and, as a consequence of the no-slip condition, where a layer of light ambient fluid penetrates below the heavy fluid. After some time, the head of the current progressively loses energy. These observations are consistent with the field and experimental data reported in Patterson *et al.* (2006) for a similar configuration. It is also important to point out that it is not possible to identify numerical spurious oscillations which seem to suggest that the present implicit LES strategy is able to capture correctly the main flow features of density currents at high Reynolds numbers.

Figure 3 presents azimuthal averaged maps as function of the vertical and radial components of the mean scalar field, the radial and vertical velocity fields, the turbulent buoyancy flux ($-\overline{u'_2\theta'}$) and the turbulent kinetic energy ($\overline{u'_i u'_i}/2$) for $t = 6.24$ and $t = 15.36$. First of all, it can clearly be seen that the maximum height of the current is located close to the head, where the first large coherent structure is penetrating into the light ambient fluid. It can also be seen that the current is quickly dissipating energy when comparing the data between $t = 6.24$ and $t = 15.36$. The interface between the current and the light ambient fluid is characterised by an intense turbulent flux activity first both from and to the current (at $t = 6.24$) and then mainly to the current (entrainment of ambient fluid in the current) at the top interface (in red) and from the current at the front interface (in blue) at $t = 15.36$. Most of the turbulence activity (high levels for the kinetic energy) is located at the head of the current.

Several theoretical and empirical models have been proposed to predict the evolution of the local front location and front velocity for axisymmetric density currents and different phases of spreading have been identified (Huppert & Simpson, 1980; Cantero *et al.*, 2007b): (i) an acceleration phase where the current initially at rest reaches its maximum velocity, (ii) a slumping phase with a nearly constant front velocity, (iii) an inertial phase for which the buoyancy driving force is balanced by inertia and during which the current starts to decelerate, (iv) a viscous phase for which the buoyancy driving force is balanced by viscosity. Note that the last two phases are often called self-similar phases and some models used to predict the evolution of the front for channelized and axisymmetric currents are based on a similarity solution of simplified equations of motion.

In the case of axisymmetric currents, it was found that the front location follows a power-law behaviour of the form
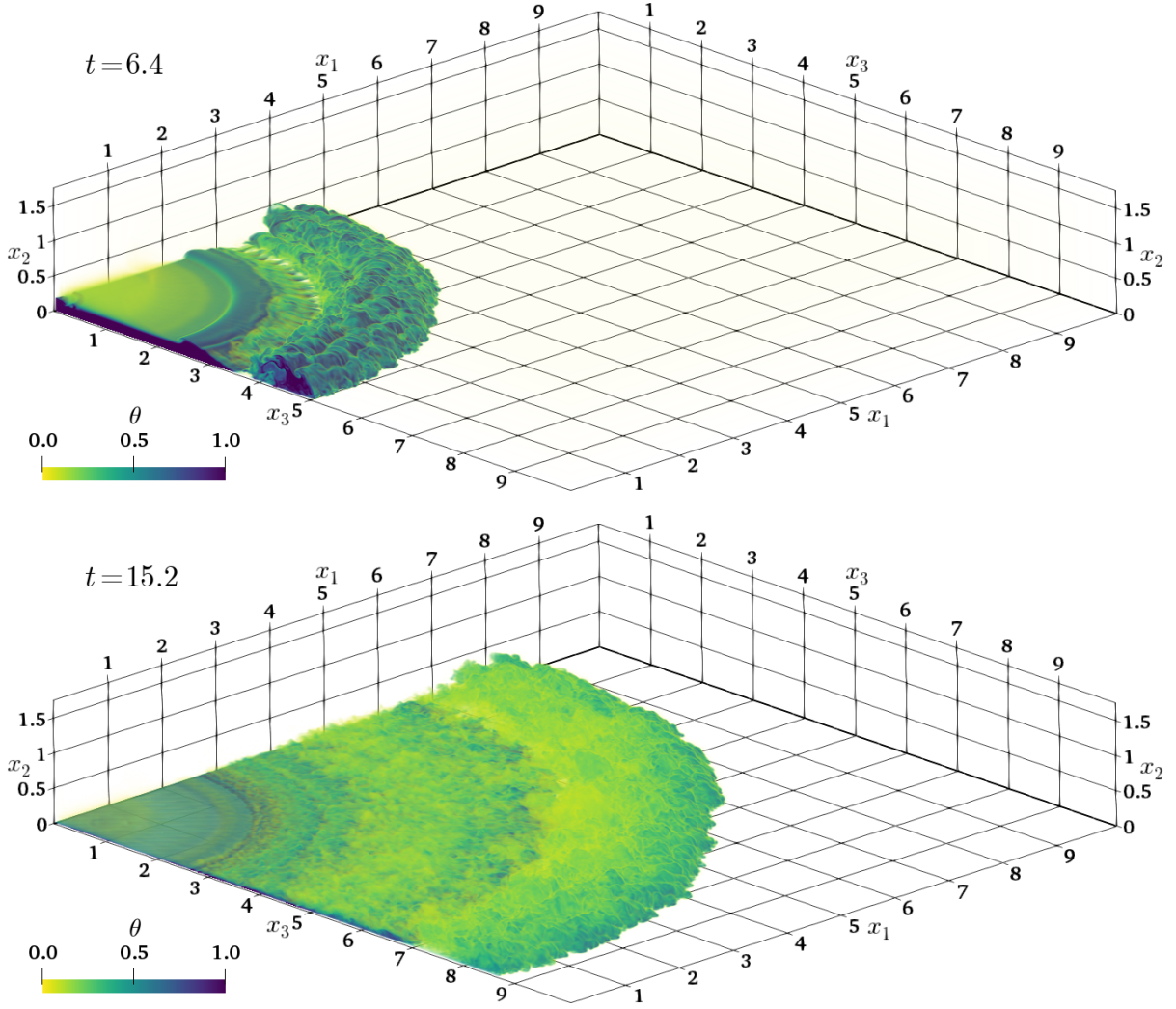
$$v_f \propto t^\alpha, \quad (7)$$

Figure 2. Instantaneous flow visualisations by volume rendering of the scalar field at Re = 136,000, at $t = 6.4$ (top) and $t = 15.2$ (bottom).

with $\alpha = -1/2$ in the inertial regime and $\alpha = -7/8$ in the viscous regime of axisymmetric currents (Huppert & Simpson, 1980; Ungarish, 2009; Cantero *et al.*, 2007*b*). The corresponding power-law for the temporal radial evolution of the front location is given by

$$r_f \propto t^{1+\alpha}. \tag{8}$$

The temporal radial evolution of the front location is presented in figure 4a. A fairly good agreement can be seen with the experimental data of Hallworth *et al.* (2001). It is reasonable to assume that the discrepancy is associated with the slightly higher initial mass, which generates a higher acceleration in the slumping phase. It can be noted that after the slumping phase, both experiment and simulation data follow the same trend. The temporal evolution of the radial front velocity is presented in figure 4b. It has been derived from the radial front position of the current. As expected, the present simulation depicts the expected characteristic phases of spreading: an initial rapid acceleration, a very short constant-velocity slumping phase, which transition to a self-similar inertial-buoyant regime in which the front moves at $v_f \propto t^{-1/2}$ followed by a viscous regime with $v_f \propto t^{-7/8}$. It should also be noted that the agreement with

the experimental data of Hallworth *et al.* (2001) is quite good, suggesting that the present implicit LES approach is suitable for reproducing the behaviour of the front location of density currents at high Reynolds numbers.

The temporal evolution of the different energy components can be extremely helpful to better understand the flow dynamics of density currents and can also be used to assess the quality of the present simulation. The conceptual framework introduced by Winters *et al.* (1995); Necker *et al.* (2002) is used to study the temporal evolution of the energy budget, and in particular the potential to kinetic energy transformation. The kinetic and potential energy are defined as

$$E_k = \frac{1}{2}\langle u_i u_i\rangle \quad \text{and} \quad E_p = \langle u_i\theta\rangle \tag{9}$$

where $u_i$ (i=1,2,3) are the velocity fields and $\theta$ is the scalar field. $\langle\bullet\rangle$ denotes an integral over the full computational domain. The dissipation rate is defined as

$$\varepsilon_T = -\frac{1}{Re}\left\langle u_j\frac{\partial^2 u_i}{\partial x_j\partial x_j}\right\rangle, \tag{10}$$
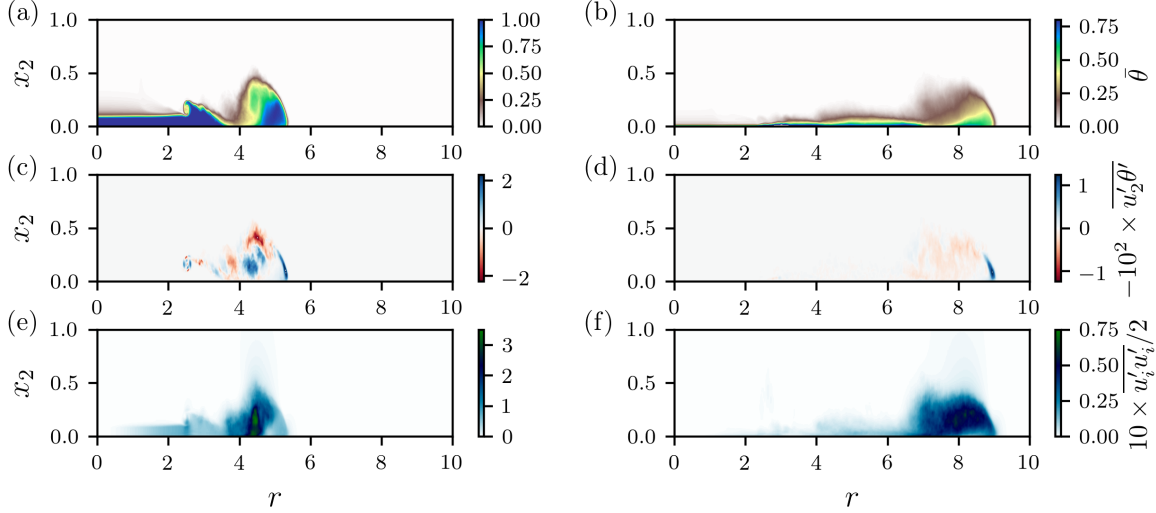
4

Figure 3. Azimuthal average maps for the scalar field (a/b), the radial velocity field (c/d), the vertical velocity field (e/f), the turbulent buoyancy flux (g/h) and the turbulent kinetic energy (i/j). Left column corresponds to $t = 6.24$ and right column to $t = 15.36$.
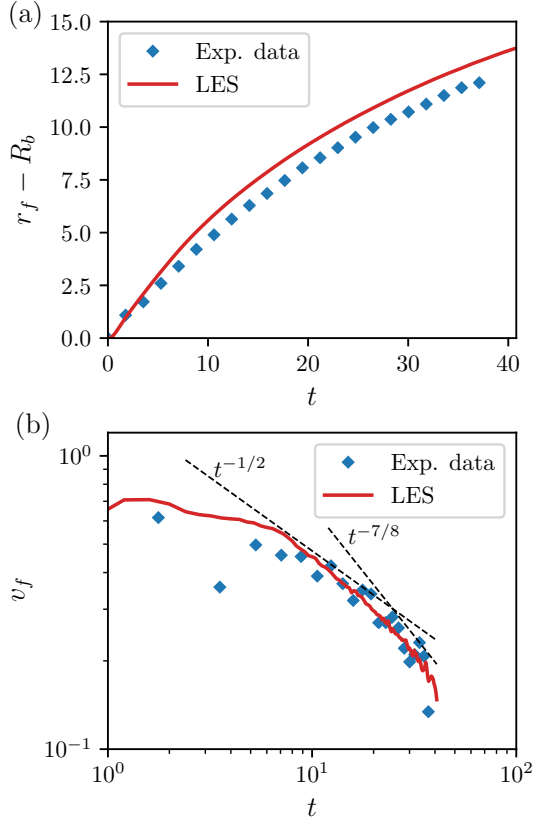


Figure 4. Temporal evolution of the radially averaged front position (a) and front velocity (b) as function of time.

and the dissipation rate associated with the scalar field is defined as

$$\Phi = -\frac{1}{ReSc}\left\langle x_2 \frac{\partial^2 \theta}{\partial x_i \partial x_i}\right\rangle. \quad (11)$$

In this framework, it can be written that

$$E_k + E_p + \underbrace{\int_0^t (\varepsilon_T + \Phi)d\tau}_{E_I} = E_{p,0}, \quad (12)$$

where $E_{p,0}$ is the total energy available in the computational domain at the start of the simulation.
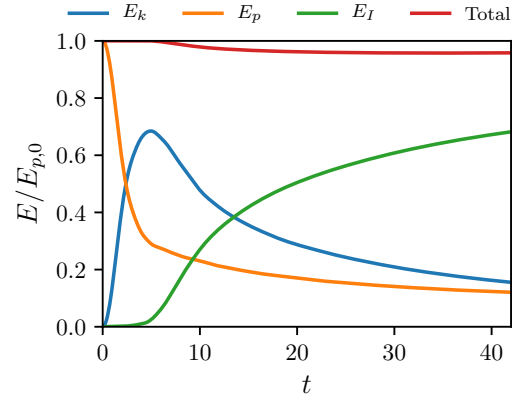


Figure 5. Energy budget normalised by the initial potential energy as function of time.

Figure 5 presents the global energy budget for the present simulation. It should be noted that the total amount of energy is not equal to 1 for the duration of the simulation likely because of the numerical dissipation introduced in our approach. The temporal evolution of the energy budget is potentially a good way to quantify the amount of numerical dissipation introduced in the simulation and this is something to investigate carefully in future studies. As in simulations at smaller Reynolds numbers (Espath *et al.*, 2014, 2015), a rapid conversion of potential energy into kinetic energy can be observed with a peak at $t \approx 5$ (over 60% of the total energy is converted into kinetic energy). When the

current is entering the inertial phase ($v_f \propto t^{-1/2}$), at $t \approx 9$, there is a rapid increase in physical dissipation, associated with a rapid decrease of kinetic energy. Towards the end of the simulation for $t > 40$, there is still about 20% of kinetic energy available to the system, suggesting that the current is still expending radially (in a self-similar fashion).

## CONCLUSION

An original scale-resolving simulation of an axisymmetric density current at a Reynolds number equal to $136,000$ was presented in this paper. The proposed numerical strategy is based on the concept of Spectral Vanishing Viscosity and seems to be perfectly capable of reproducing (at no extra cost) the main features of density currents at high Reynolds numbers (for which experimental data are available). This is a very encouraging result which will pave the way for future numerical studies of density currents at realistic Reynolds numbers.

## ACKNOWLEDGEMENTS

## REFERENCES

Cantero, Mariano I, Balachandar, S & Garcia, Marcelo H 2007*a* High-resolution simulations of cylindrical density currents. *J. of Fluid Mechanics* **590**, 437–469.

Cantero, Mariano I, Balachandar, S, García, Marcelo H & Ferry, James P 2006 Direct numerical simulations of planar and cylindrical density currents. *J. of Applied Mechanics* **73** (6), 923–930.

Cantero, Mariano I, Lee, JR, Balachandar, S & Garcia, Marcelo H 2007*b* On the front velocity of gravity currents. *J. of Fluid Mechanics* **586**, 1–39.

Constantinescu, George 2014 LES of lock-exchange compositional gravity currents: a brief review of some recent results. *Environmental Fluid Mechanics* **14** (2), 295–317.

Dairay, Thibault, Lamballais, Eric, Laizet, Sylvain & Vassilicos, John Christos 2017 Numerical dissipation vs. subgrid-scale modelling for large eddy simulation. *J. of Computational Physics* **337**, 252–274.

Deskos, Georgios, Laizet, Sylvain & Piggott, Matthew D 2019 Turbulence-resolving simulations of wind turbine wakes. *Renewable Energy* **134**, 989–1002.

Espath, L.F.R., Pinto, L.C., Laizet, S. & Silvestrini, J.H. 2014 Two- and three-dimensional direct numerical simulation of particle-laden gravity currents. *Computers & Geosciences* **63**.

Espath, LFR, Pinto, LC, Laizet, S & Silvestrini, JH 2015 High-fidelity simulations of the lobe-and-cleft structures and the deposition map in particle-driven gravity currents. *Physics of Fluids* **27** (5), 056604.

Hallworth, Mark A., Huppert, Herbert E. & Ungarish, Marius 2001 Axisymmetric gravity currents in a rotating system: experimental and numerical investigations. *J. of Fluid Mechanics* **447**, 129.

Härtel, C., Carlsson, F. & Thunblom, M. 2000*a* Analysis and direct numerical simulation of the flow at a gravity-current head. Part 2. The lobe-and-cleft instability. *J. of Fluid Mechanics* **418**, 213–229.

Härtel, C., Meiburg, E. & Necker, F. 2000*b* Analysis and direct numerical simulation of the flow at a gravity-current head. Part 1. Flow topology and front speed for slip and no-slip boundaries. *J. of Fluid Mechanics* **418**, 189–212.

Huppert, H.E. & Simpson, J.E. 1980 The slumping of gravity currents. *J. of Fluid Mechanics* **99(04)**, 785–799.

Ioannou, Vasilis & Laizet, Sylvain 2018 Numerical investigation of plasma-controlled turbulent jets for mixing enhancement. *Int. J. of Heat and Fluid Flow* **70**, 193–205.

Karamanos, G.S. & Karniadakis, G.E. 2000 A spectral vanishing viscosity method for Large-Eddy Simulations. *J. of Computational Physics* **163** (1), 22–50.

Laizet, S. & Lamballais, E. 2009 High-order compact schemes for incompressible flows: A simple and efficient method with the quasi-spectral accuracy. *J. of Computational Physics* **228**, 5989–6015.

Laizet, Sylvain & Li, Ning 2011 Incompact3d: A powerful tool to tackle turbulence problems with up to $0(10^5)$ computational cores. *Int. J. for Numerical Methods in Fluids* **67** (11), 1735–1757.

Lamballais, Eric, Fortuné, Véronique & Laizet, Sylvain 2011 Straightforward high-order numerical dissipation via the viscous term for direct and large eddy simulation. *J. of Computational Physics* **230** (9), 3270–3275.

Lele, Sanjiva K 1992 Compact finite difference schemes with spectral-like resolution. *J. of Computational Physics* **103** (1), 16–42.

Meiburg, Eckart & Kneller, Ben 2010 Turbidity currents and their deposits. *Annual Review of Fluid Mechanics* **42**, 135–156.

Necker, F., Hartel, C., Kleiser, L. & Meiburg, E. 2002 High-resolution simulations of particle-driven gravity currents. *Int. J. of Multiphase Flow* **28**, 279–300.

Patterson, Michael D, Simpson, JE, Dalziel, SB & Van Heijst, GJF 2006 Vortical motion in the head of an axisymmetric gravity current. *Physics of fluids* **18** (4), 046601.

Simpson, John E 1999 *Gravity currents: In the environment and the laboratory*. Cambridge university press.

Ungarish, M. 2009 *An introduction to gravity currents and intrusions*. CRC Press.

Winters, Kraig B., Lombard, Peter N., Riley, James J. & D'Asaro, Eric A. 1995 Available potential energy and mixing in density-stratified fluids. *J. of Fluid Mechanics* **289**, 115128.

Zgheib, N., Bonometti, T. & Balanchandar, S. 2015 Direct numerical simulation of cylindrical particle-laden gravity currents. *Computers & Fluids* **123**, 23–31.